ISSN 1070-3284, Russian Journal of Coordination Chemistry, 2013, Vol. 39, No. 5, pp. 379–387. © Pleiades Publishing, Ltd., 2013.
Original Russian Text © P.A. Abramov, M.N. Sokolov, I.V. Mirzaeva, N.K. Moroz, 2013, published in Koordinatsionnaya Khimiya, 2013, Vol. 39, No. 5, pp. 271–280.

Synthesis, NMR and Quantum Chemical Studies of the $[Cp_3Rh_3Se_2]^{2+}$ Clusters (Cp = η^5-C_5Me_5, η^5-C_5Me_4Et, η^5-$C_5H_3{}^tBu_2$)[1]

P. A. Abramov[a, b, *], M. N. Sokolov[a, b], I. V. Mirzaeva[a], and N. K. Moroz[a]

[a] *Nikolayev Institute of Inorganic Chemistry SB RAS, Novosibirsk, 630090 Russia*

[b] *Novosibirsk State University, Novosibirsk, 630090 Russia*

**e-mail: abramov@niic.nsc.ru*

Received October 15, 2012

Abstract—Reactions of $[CpRhCl_2]_2$ (Cp = η^5-C_5Me_5 (Cp*), η^5-C_5Me_4Et (Cp'), η^5-$C_5H_3{}^tBu_2$ (Cp")) with in situ generated H_2Se give triangular $[Cp_3Rh_3Se_2]^{2+}$ clusters. These clusters were isolated as PF_6 salts and characterized with ESI–MS, ^{77}Se, ^1H NMR and DFT calculations. $[Cp_3Rh_3Se_2]$ undergoes two reversible two-electron reduction steps. Quantum-chemical calculations reveal non-trivial bonding situation in the cluster core and changes in the hapticity of the Cp* ligand upon reduction. Crystal structure of $[Cp^*_3Rh_3Se_2][Re_2(\mu\text{-}Cl)_3(CO)_6]Cl \cdot 3.3H_2O$ has been determined.

DOI: 10.1134/S1070328413050011

INTRODUCTION

Our interest in these compounds is related to the reported activity of the sulfide clusters $[Cp_3M_3Q_2]^{2+}$ (M = Co, Rh, Ir) [1–3] in electrochemical CO_2 reduction: electrochemical reduction of $[Cp^*_3M_3(\mu_3\text{-}S)_2]^{2+}$ in CO_2–saturated CH_3CN at –1.3 V (vs. Ag/AgCl) produced $C_2O_4^{2-}$ and $[Cp^*_3Ir_2(Ir(\eta^4\text{-}C_5Me_5)CH_2CN)(\mu_3\text{-}S)_2]^+$ [3]. Triangular $[Cp^*_3M_3Se_2]^{2+}$ (M = Rh, Ir) clusters were initially prepared in reactions of $[Cp^*MCl_2]_2$ (M = Rh, Ir) with H_2Se (generated from Al_2Se_3 and H_2O–CH_2Cl_2, 48–72 h). Another way of making $[Cp^*_3M_3Se_2]^{2+}$ is to react $[Cp^*_3M_2(\mu\text{-}SeH)_2Cl_2]$ with $[Cp^*MCl_2]_2$ [4]. These reactions are run under mild conditions. We have found that under drastic conditions (140°C, 48 h) H_2Se generated in situ from ZnSe and 4 M HCl reacts with $[(C_5Me_4Et)Rh(C_6H_6)](PF_6)_2$ with the formation of $[(C_5Me_4Et)_3M_3(\mu_3\text{-}Se)_2]^{2+}$ in high yield, the arene ligand being the leaving group [5]. To explore the possibility of formation of other selenidation products, in this work we studied reactions of $[CpRhCl_2]_2$ (Cp = η^5-C_5H_5 (Cp*), η^5-C_5Me_5Et (Cp'), η^5-$C_5H_3{}^tBu_2$ (Cp")) with in situ generated H_2Se under the same conditions (4 M HCl, 140°C, 48 h). In all cases the $[Cp_3Rh_3(\mu_3\text{-}Se)_2]^{2+}$ clusters were found to be the only or main products, according to ESI–MS and NMR spectra.

EXPERIMENTAL

All syntheses were run in sealed glass tubes (h = 150 mm, d = 10 mm). H_2Se was generated from ZnSe and 4 M HCl upon heating. All manipulations were done in a fume cupboard because of high toxicity of H_2Se. $[Cp^*RhCl_2]_2$ and $[Cp"RhCl_2]_2$ were prepared by the published procedures [6]. $[Cp'_3Rh_3Se_2](PF_6)$ was synthesized as described (UV–VIS of $[Cp'_3Rh_3Se_2]^{2+}$ in 4 M HCl: λ_{max} = 232, 265(sh), 338(sh), 408 nm) [5]. CH_3CN and CH_2Cl_2 were distilled over P_2O_5.

Synthesis of $[Cp^*_3Rh_3Se_2](PF_6)_2$ (I). 0.1 g (0.16 mmol) of $[Cp^*RhCl_2]_2$ and 0.14 g (1.00 mmol) of ZnSe in 2 mL of 4 M HCl were placed into a glass tube which was evacuated and flame-sealed. Heating for 48 h at 140°C gave a dark-red solution and a black precipitate. The precipitate was filtered off and dried in vacuo. ESI–MS spectra of methanol extracts showed the presence of $[Cp^*_3Rh_3Se_2]^{2+}$ (major peak) and of $[Cp^*_4Rh_4Se_4]^{2+}$ (m/z = 634, minor peak). The filtrate was evaporated and extracted with water. The ^1H NMR spectra of the extract showed only one signal at 2.02 ppm from $[Cp^*_3Rh_3Se_2]^{2+}$. NH_4PF_6 (0.1 g) was added to the dark-red solution to produce dark-red precipitate of $[Cp^*_3Rh_3Se_2](PF_6)_2$. The crude product

[1] The article was translated by the authors.

was extracted with 3 mL of CH_3CN. Single crystals were obtained by crystallization from a CH_3CN/Et_2O mixture, crystallographic parameters were the same as reported in [4]. Yield 54 mg (50%). ^1H NMR (r.t., $CDCl_3$, δ, ppm): 2.02. ESI–MS (*m/z*, $CDCl_3$): 436 (M^{2+}).

For $C_{30}H_{45}F_{12}P_2Se_2Rh_3$		
anal. calcd., %:	C, 31.0;	H, 3.9.
Found, %:	C, 31.3;	H, 4.0.

Synthesis of $[Cp''_3Rh_3Se_2](ZnCl_4)$ (II): 0.025 g (0.037 mmol) of $[Cp''RhCl_2]_2$ and 0.02 g (0.14 mmol) of ZnSe in 2 mL of 4 M HCl were reacted under the same conditions as above to give a dark-violet precipitate and a colorless solution. The precipitate was filtered and extracted with 3 mL CH_2Cl_2. Evaporation of the extract gave 0.028 mg of dark-red powder. Yield 74%. ESI–MS(+) (*m/z*, CH_2Cl_2): $[Cp''_3Rh_3Se_2]^{2+}$ ($m/z = 500$), $[Cp''_3Rh_3Se_2]^+$ ($m/z = 1000$).

For $C_{27}H_{39}Cl_4Se_2ZnRh_3$		
anal. calcd., %:	C, 38.8;	H, 5.3.
Found, %:	C, 39.2;	H, 5.0.

Synthesis of $[Cp^*_3Rh_3Se_2][Re_2(\mu\text{-}Cl)_3(CO)_6]Cl \cdot 3.3H_2O$ (III): 0.07 g (0.1 mmol) of $[Cp^*RhCl_2]_2$, 0.041 g (0.1 mmol) of $[Re(CO)_5Br]$ and 0.1 g (0.7 mmol) of ZnSe in 2 mL of 4 M HCl were reacted under the same conditions as above to give a red solution and a brown precipitate. UV–VIS spectra of the solution indicated formation of $[Cp^*_3Rh_3Se_2]^{2+}$ [5]. The brown precipitate was filtered off, dried in air and extracted with methanol. Thick red crystals of **III** were obtained by evaporation of methanolic solution in a narrow tube. Yield: 15 mg. IR (KBr, ν, cm^{-1}): 3427(w), 3196(w), 2020(s), 1897(s). ESI–MS(+) (*m/z*, CH_3OH): 436 (M^{2+}), ESI–MS(–) (*m/z*, CH_3OH: 341 ($[ReCl(CO)_3]^-$), 646 ($[Re_2(\mu\text{-}Cl)_3(CO)_6]^-$).

NMR. ^{77}Se NMR spectra of $[Cp^*_3Rh_3Se_2](PF_6)_2$ and $[Cp'_3Rh_3Se_2](PF_6)_2$ in $CDCl_3$ were recorded with a Bruker Avance 500 spectrometer operating at 95.38 MHz at room temperature. The ^{77}Se chemical shifts were referenced to H_2SeO_3 (δ = 1282 ppm) as external standard, and then recalculated vs. $SeMe_2$ (δ = 0 ppm). Total range of ^{77}Se shifts from –1000 to 2000 ppm was scanned.

DFT calculations. Geometries of $[Cp^*_3Rh_3Se_2]^{2+}$, and $[Cp'_3Rh_3Se_2]^{2+}$ cations and of the reference molecules $SeMe_2$ and H_2SeO_3 were optimized with ADF 2008 program [7]. We used zero order regular approximation (ZORA) [8] to account for scalar relativistic effects together with BP density functionals [9–11]. The basis set consisted of relativistic Slater type orbitals of triple–ζ quality augmented with a set of polarized orbitals (TZP/ADF). To speed up geometry optimization, inner atomic shells were treated with frozen core approximation (Rh—3*d*; Se—3*p*; C—1*s*). NMR shieldings were calculated with DFT–GIAO method [12]. To characterize chemical bonding we used topological analysis of electron density ρ(*r*) (AIM theory by R. Bader [13]) and Electron Localization Function (ELF) [14, 15]. Atoms are represented by regions of real space around ρ(*r*) local maxima separated by gradient of ρ(*r*) zero flux surfaces. Interatomic interactions (i.e. chemical bonds) are represented by bond paths and bond critical points (BCP). BCP properties (values of ρ(*r*), Δρ(*r*), potential energy density *V*(*r*) and kinetic energy density *G*(*r*) at BCP) characterize nature of the bond (ionic, covalent, van der Waals, etc.). When bond paths form a closed ring, in the center of the ring there appears a ring critical point (RCP). Some works associate RCP properties with multicenter bonding in aromatic systems [16, 17], but up to now there have been no such works for transition metal clusters. Cage critical points (CCP) correspond to local minima of electron density.

Electron Localization Function analysis offers a more developed concept of multicenter bonding [18], in particular for transition metal complexes [19–21]. Topological analysis of ELF allows partitioning of the real space into chemically meaningful regions: core electrons, lone pairs, and covalent bonds. Values of ELF are unitless. The upper limit of ELF = 1 corresponds to perfect localization of the electrons, and the value of ELF = 0 means that no electrons are localized at this point. Since ELF is a scalar function, analysis of its gradient field must be carried out in order to locate its *attractors* (local maxima) and corresponding *basins* (regions around attractors that contain all ELF gradient trajectories ending at a particular attractor). *Core basins* (surrounding nuclei) are denoted as C(A) where A stands for the atomic symbol of the atom to which it belongs. V(A, B, ..., X) denotes a *valence basin* shared by atomic centers A, B, ..., X. Multicenter interactions are represented by valence basins that border more than two core basins.

Crystallography. Crystallographic data and refinement details are given in Table 1. The diffraction data were collected on a Bruker ApexDUO CCD diffractometer with CuK_α radiation (λ = 1.54 Å) by doing φ and ω scans of narrow (0.5°) frames at 100 K. Structure of **III** was solved by direct methods and refined by full-matrix least-squares treatment against $|F|^2$ in anisotropic approximation with SHELXTL programs set [22]. Absorption corrections were applied empirically with SADABS program [23]. All nonhydrogen atoms of main structural units were refined anisotropically. The hydrogen atoms were refined in their geometrically calculated positions; a riding model was used for this purpose. The Cl^- anion and water molecules were found to be disordered over few positions with small

occupations, due to these atoms were refined in isotropic approximation, while the hydrogen atoms of water molecules were not localized. Further details may be obtained from the Cambridge Crystallographic Data Center on quoting the depository number CCDC 874012. Copies of this information may be obtained free of charge from http://www.ccdc.cam.ac.uk.

RESULTS AND DISCUSSION

Synthesis and NMR. Interaction of $[Cp'RhCl_2]_2$ with H_2Se under drastic conditions (140°C, 48 h) gives triangular clusters $[Cp'_3Rh_3Se_2]^{2+}$ as the only Se-containing products in high yields in almost all cases, with minor amounts of $[Cp'Rh(\mu\text{-}Cl)_3RhCp'](PF_6)_2$ as by-products [2]. Only in the case of Cp = Cp* formation of a cuboidal cluster, $[Cp^*_4Rh_4Se_4]^{2+}$ was detected by ESI–MS, as minor product. With bulky η^5-$C_5H_3{}^tBu_2$ (Cp'') substituent only formation of the triangular cluster was observed. In an earlier work [24] we reported that reaction of $[Re(CO)_5Br]$ with in situ generated H_2Se gave rise to two polyselenide complexes $[Re(CO)_3(H_2O)_3][Re_5(CO)_{18}(Se_2)_3]$ and $[Re_4(CO)_{14}(Se_2)(Se_5)]$. Attempts to introduce a heterometal (Re) by carrying out this reaction in the presence of $[Re(CO)_5Cl]$ gave only double complex salt $[Cp^*_3Rh_3Se_2][Re_2(\mu_3\text{-}Cl)_3(CO)_6]Cl \cdot 3.3H_2O$ (**III**). These results reveal that the $\{Rh_3Se_2\}$ clusters must be thermodynamically preferred species, the $\{Rh_3Se_2\}^{2+}$ core being remarkably robust even in hot highly acidic media; and that selenidation of $\{CpRh\}^{2+}$ moiety is favored over that of isoelectronic $\{Re(CO)_3\}^+$ moiety. Crystal structure of **III** (Fig. 1) consists of the cationic clusters $[Cp^*_3Rh_3(\mu_3\text{-}Se)_2]^{2+}$, binuclear Cl-bridged rhenium(I) carbonylates $[Re_2(\mu_3\text{-}Cl)_3(CO)_6]^-$ and highly disordered Cl^- anions and water molecules. Geometrical parameters of the cluster core in **III** (Rh–Rh 2.887(2) Å, Rh–Se 2.390(2) Å) are very close to those reported for **I** [4] and $[Cp'_3Rh_3(\mu_3\text{-}Se)_2]^{2+}$ [5].

Table 1. Experimental details

Parameter	Value
Chemical formula	$C_{36}H_{51.60}O_{9.30}Cl_4Se_2Rh_3Re_2$
M	1614.02
Crystal system	Hexagonal
Space group	$P6_3/m$
Temperature, K	100
a, Å	14.0939 (3)
c, Å	15.6298 (8)
V, Å^3	2688.72 (16)
Z	2
$F(000)$	1526
μ, mm^{-1}	19.59
Crystal size, mm	0.30 × 0.05 × 0.03
Absorption correction	Multi-scan Bruker SADABS
T_{min}, T_{max}	0.066, 0.630
No. of measured, independent and observed ($I > 2\sigma(I)$) reflections	5440, 1625, 1222
R_{int}	0.033
θ_{min}, θ_{max}, deg	5.7, 67.6
Range of h, k, l	$-16 \le h \le 12$, $-12 \le k \le 16$, $-18 \le l \le 3$
R ($F^2 > 2\sigma(F^2)$), $wR(F^2)$, S	0.077, 0.234, 1.14
No. of reflections, parameters, restraints	100
Weight scheme	$w = 1/[\sigma^2(F_o^2) + (0.1169P)^2 + 43.2445P]$, where $P = (F_o^2 + 2F_c^2)/3$
$\Delta\rho_{max}$, $\Delta\rho_{min}$, e Å^{-3}	2.08, −1.37

Note: Computer programs: APEX2 (Bruker-AXS, 2004), SAINT (Bruker-AXS, 2004), SHELXS-97 (Sheldrick, 1998), SHELXL-97 (Sheldrick, 1998), SHELXTL (Bruker-AXS, 2004), CIFTAB-97 (Sheldrick, 1998).

^{77}Se NMR spectrum of **I** in CD_3CN at room temperature shows only one peak centered at 1685.46 ppm (Fig. 2a), which is much more downfield than hitherto reported shifts for Se in a μ_3-position [25, 26]. The peak is rather broad (19 Hz halfwidth). This may be explained with the fact that ^{77}Se NMR shifts are very sensitive to the environment, and in the case of **I** different orientations of the Cp* groups may affect the shift value. Rotation of these groups around C_5 axes generates equally possible Cp* orientations and causes peak broadening. We tried heating the sample to see if the peak narrows due to a Cp* reorientation process around the C_5 symmetry axes and found that up to 315 K the peak width remained the same but its position shifted slightly, to 1683.31 ppm. No splitting due to ^{103}Rh–^{77}Se spin–spin coupling interaction was observed. That means that direct ^{103}Rh–^{77}Se spin–spin coupling constant does not exceed 19 Hz.

^{77}Se NMR spectrum of $[Cp'_3Rh_3Se_2](PF_6)_2$ in CD_3CN at room temperature shows two resonances, at 1689.88 ppm and at 1688.62 ppm (Fig. 2b), with halfwidths of 19.4 Hz and 18.5 Hz, respectively. This difference of only 1.26 ppm is rather small for ^{77}Se NMR shifts scale. We assume that in solution there are two relatively stable conformers of $[Cp'_3Rh_3Se_2]^{2+}$ only differing in relative orientations of the Et groups of the C_5Me_4Et ligands (oriented towards the center of the complex or away from it).

After geometry optimization the Rh–Rh and Rh–Se distances in the $[Cp^*_3Rh_3Se_2]^{2+}$ and a $[Cp'_3Rh_3Se_2]^{2+}$

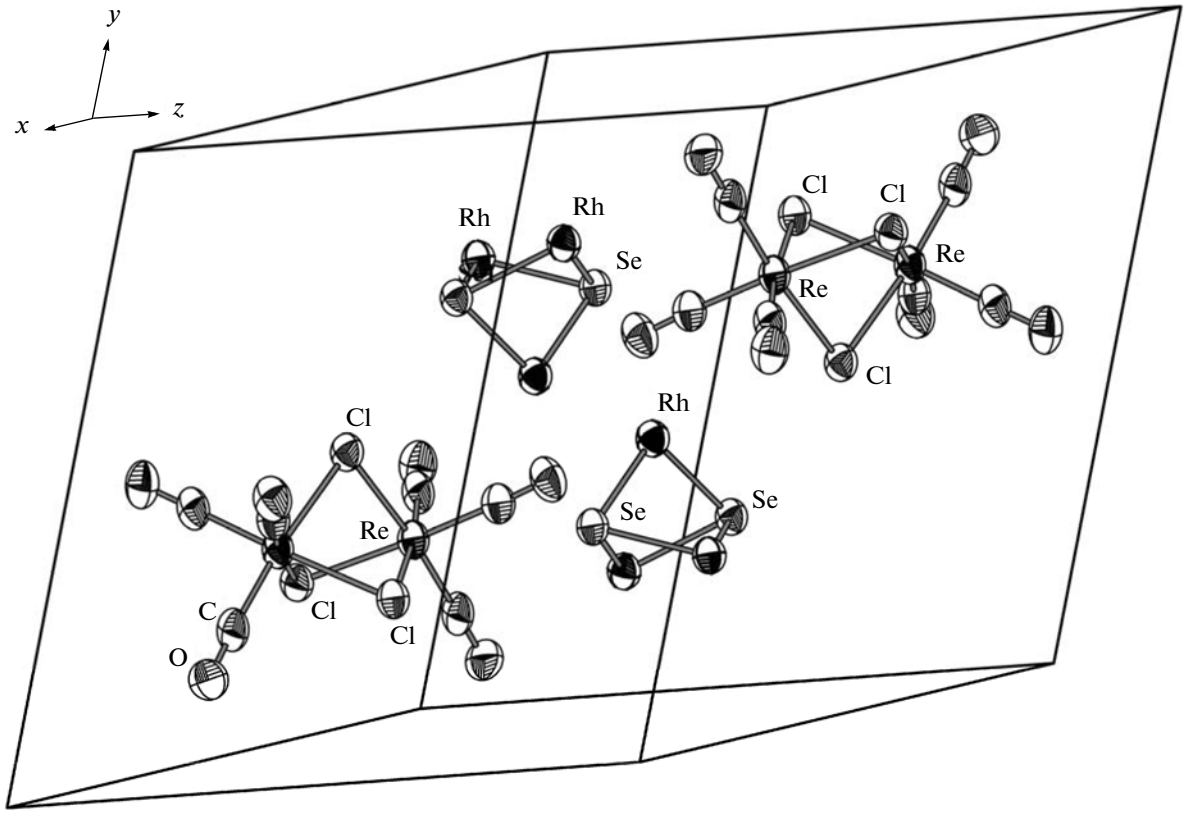

Fig. 1. Unit cell of **III** (ellipsoids of 50% probability). Cp* ligands and disordering Cl- and water molecules are not shown for clarity.

clusters (Table 2) were slightly longer than the experimental values obtained from X-ray structure analysis (2.88 and 2.40 Å, respectively) [4, 5]. The structure of $[Cp^*_3Rh_3Se_2]^{2+}$ was optimized in C_{3v} symmetry, while $[Cp'_3Rh_3Se_2]^{2+}$ had no symmetry. As a result, the three Rh...Rh distances in $[Cp'_3Rh_3Se_2]^{2+}$ were slightly non-equivalent. All the Rh–Se distances were found to be the same (2.43 Å) in both cations. Nevertheless, different positions of Cp* and Cp' make two Se atoms magnetically non-equivalent, which is reflected by noticeable differences in calculated values of the ^{77}Se NMR shifts (Table 3), higher than experimental peak widths. Calculated NMR shifts for ^{77}Se nuclei are higher than the experimental values (Table 3). There may be several reasons for that. Apart from errors that are inherent in the model simplifications in electron structure calculations, the difference between real and optimized interatomic distances may be too large. Another reason is that our calculations do not take into account atomic vibrations. Temperature dependence of the peak shift in $[Cp'_3Rh_3Se_2]^{2+}$ supports the latter argument. Calculated ^{103}Rh–^{77}Se spin–spin coupling constants are ~13 Hz, in agreement with the absence of splitting satellites in observed NMR signals.

Table 2. Selected distances for optimized geometries of $[Cp^*_3Rh_3Se_2]^{2+}$, $[Cp'_3Rh_3Se_2]^{2+}$ and neutral $[Cp^*_3Rh_3Se_2]$

Bond, Å	$[Cp^*_3Rh_3Se_2]^{2+}$	$[Cp'_3Rh_3Se_2]^{2+}$	$[Cp^*_3Rh_3Se_2]^{0}$
Rh–Rh	2.95	2.94, 2.96, 2.97	2.83, 2.86, 3.69
Rh–Se	2.43	2.43	2.46, 2.44, 2.44
Rh–C	2.22–2.25	2.21–2.26	2.19–3.35

Electronic structure. Both systems ($[Cp'_3Rh_3Se_2]^{2+}$ and $[Cp^*_3Rh_3Se_2]^{2+}$) show similar bonding structure (Fig. 3a). Curiously, there are weak long-distance contacts between the hydrogen atoms of the Cp rings with electron density values in corresponding BCPs less then 0.002 a.u. Properties of selected electron density critical points are shown in Table 3. In this work we were interested mostly in interactions involving Rh atoms. According to Espinosa classification [27], the Rh–C and Rh–Se bonds belong to intermediate type, typical for interactions involving transition metal atoms. There are no BCPs between each pair of Rh atoms (i.e. there are no direct Rh–Rh bonds). Instead, there are RCPs that correspond to Rh–Se–Rh–Se cycles. Negative values of electron full energy density H in the Rh–Se–Rh–Se RCPs and Rh–Rh–Rh–Se–

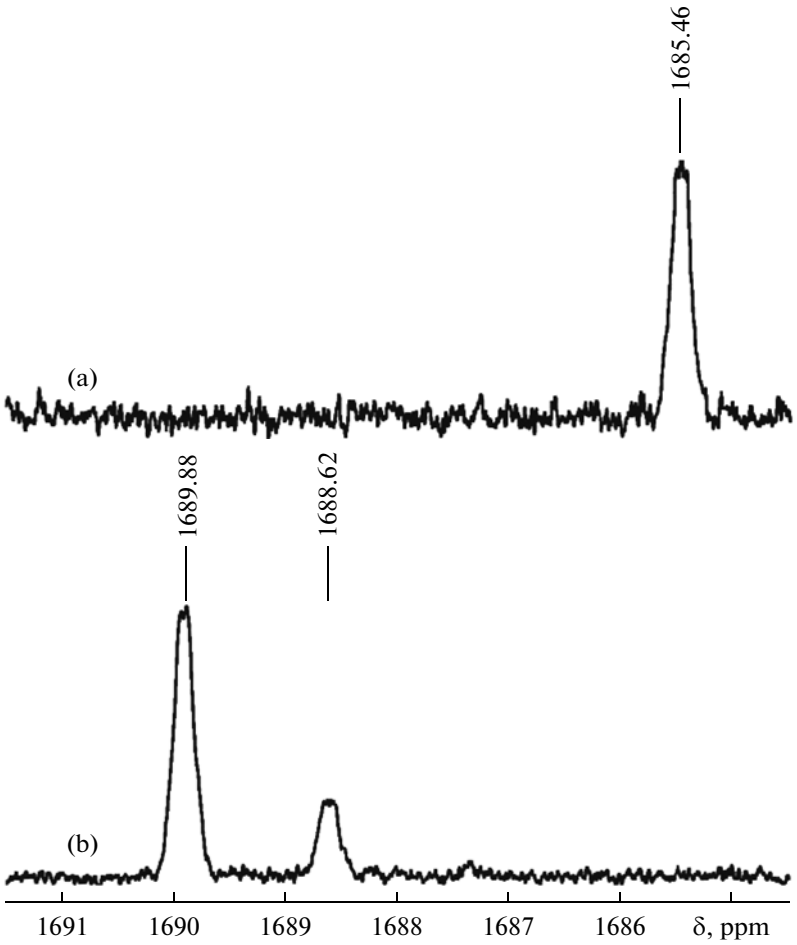

Fig. 2. ^{77}Se NMR spectra for $[Cp^*_3Rh_3Se_2](PF_6)_2$ (a) and $[Cp'_3Rh_3Se_2](PF_6)_2$ (b) in CD_3CN solution at room temperature.

Se CCP indicate that there are shared electrons in the space between Se and Rh atoms.

According to ELF classification, Se–Rh bonds are closed shell. There are unusual basins between each pair of Rh atoms (Fig. 4). These basins separate from the rest system at rather low ELF values (0.275) and have higher ELF values at saddle points on the borders with Se lone pairs than with Rh core basins. It looks like if they were connecting Se atoms rather than Rh atoms (Fig. 4). These basins are also displaced away from the Rh–Rh axis. Although these basins have to be classified as bonding Rh–Rh basins, they refer to Rh–Se–Rh–Se RCPs in AIM analysis, and, hence, represent four-center Rh–Se–Rh–Se bonding. Similar conclusions may be drawn from the analysis of highest occupied molecular orbitals (Fig. 5). The HOMO of $[Cp^*_3Rh_3Se_2]^{2+}$ is twice degenerated and contains both bonding and antibonding terms for two of the Rh–Rh contacts and only antibonding terms for the third Rh–Rh contact (Fig. 5). The HOMO^{-1} of $[Cp_3Rh_3Se_2]^{2+}$ also contains bonding and antibonding terms for two of the Rh–Rh contacts (the third pair) and only antibonding terms for the remaining Rh–Rh contact (Fig. 5). Both HOMO and HOMO^{-1} contain bonding terms for four Se–Rh bonds with the pair of Rh atoms that have only antibonding terms for the Rh–Rh contact, while for the remaining two Se–Rh contacts, the MO contains only antibonding terms. Therefore, we may conclude that the capping Se atoms donate electronic density from their lone pairs to the Rh–Rh antibonding orbitals. These complexes are

Table 3. Experimental and calculated NMR chemical shifts and Rh–Se spin coupling constants

Chemical shift	$SeMe_2$	H_2SeO_3	$[Cp^*_3Rh_3Se_2]^{2+}$	$[Cp'_3Rh_3Se_2]^{2+}$
σ_{iso}	1665	350	−185, −182	−190, −176
δ_{calc}	0	1315	1850, 1847	1855, 1841
δ_{exp}	0	1282	1685	1690, 1687

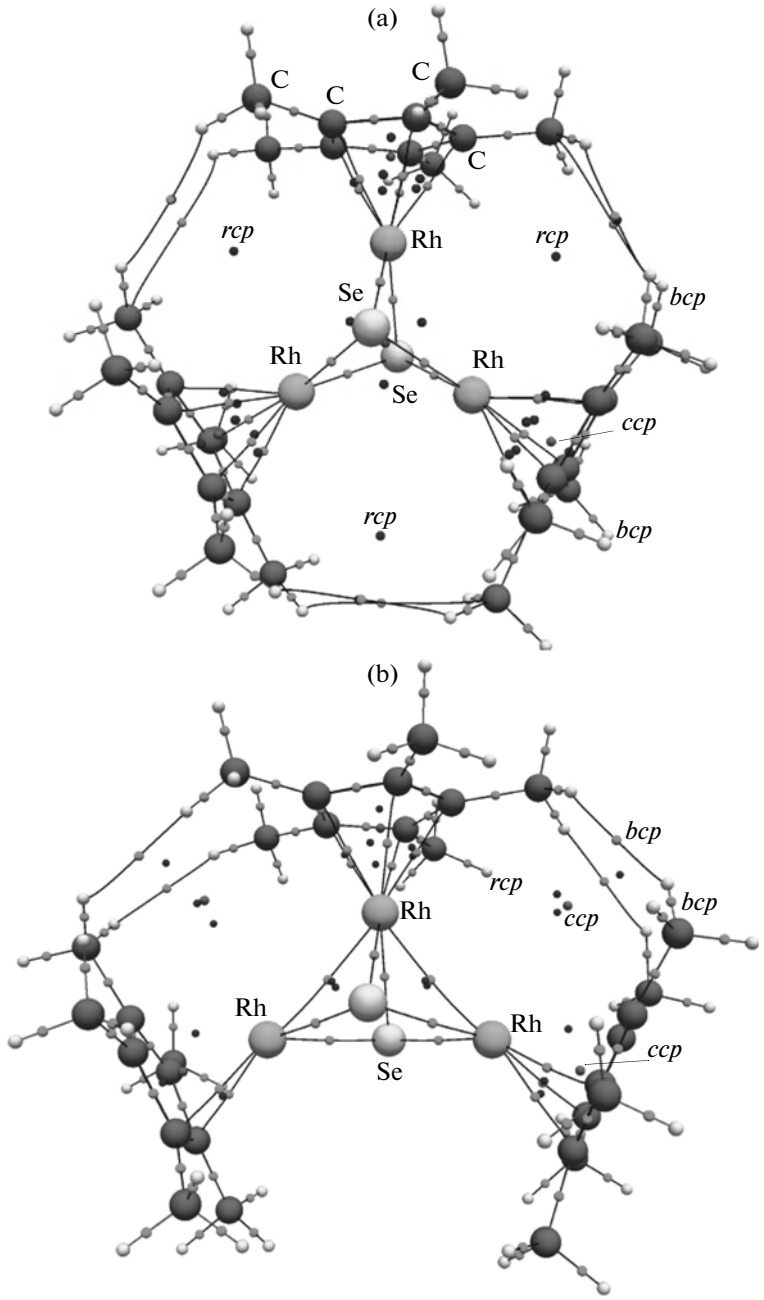

Fig. 3. Isosufrace ELF = 0.275. Blue—Rh core basins; yellow—Se valence basins (lone pairs); pink—shared Rh–Rh valence basin.

thus to be regarded not as classical triangular clusters with 48 cluster valence electrons (CVE), but (in formal description) rather as electron-rich 50 or even 52 CVE complexes with weakened Rh–Rh bonding. This extra donation helps to explain rather short Rh–Se distances (2.39–2.40 Å) found in these clusters [4, 5] which are appreciably shorter than in $[Rh_3Se_2(CO)_6]^-$ (2.46 Å) [28]. Precision determination of electronic density has shown that similar shortening of the V–S bonds (and V–V distances) observed in electron-deficient $[Cp_4V_4S_4]$ is due to increased back donation from the lone pairs centered on μ_3-S atoms [29]. Recent review by Prof. A.A. Pasynski shows that this back donation is very important in cluster complexes and often competes with metal–metal bonding [30].

The doubly reduced form $[Cp^*_3Rh_3Se_2]^0$ plays important role in electrochemical CO_2 reduction [1] We have studied electronic structure of its analogue $[Cp^*_3Ir_3S_2]^0$ by DFT calculations. The total energy of

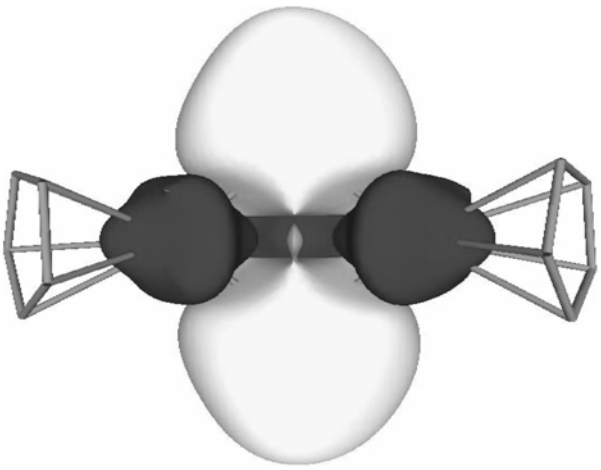

Fig. 4. Isosufrace ELF = 0.275. Very small basin of V(Rh,Rh) is depicted in comparison with core basins of Rh and Se.

optimized neutral molecule $[Cp^*_3Rh_3Se_2]^0$ was found still negative but by 12 eV higher then the total energy of $[Cp^*_3Rh_3Se_2]^{2+}$. Selected interatomic distances for $[Cp^*_3Rh_3Se_2]^0$ are shown in Table 2. Properties of selected critical points of electron density are shown in Table 4. The main difference between $[Cp^*_3Rh_3Se_2]^{2+}$ and $[Cp^*_3Rh_3Se_2]^0$ resides is the *formation* of two Rh–Rh bonds (which is reflected by shortening of Rh–Rh distance by 0.1 Å, Table 2) accompanied with the *displacement* of two Cp* rings, which opens the opportunity for other chemical groups to coordinate two Rh atoms and become activated (Fig. 3b). Corresponding to Rh–Rh bonds electron density in BCPs is slightly higher in Rh–Se–Rh–Se RCPs. According to Rh–Se distances and electron density values in Rh–Se BCPs, it is the Rh atom involved in both Rh–Rh bonds that forms weakest Rh–Se bonds. Three Rh atoms and two Se atoms do not form cage structure. All Cp*–Rh fragments form cages with just a little bit lower values of electron density in CCPs. One of the Cp* rings has two direct Rh–C bonds (η^2) and another one has three Rh–C bonds (η^3). Properties of all RCPs in the center of Cp* and Rh–C–C BCPs are very similar to those in $[Cp^*_3Rh_3Se_2]^{2+}$.

This work shows that the formation of $[Cp^*_3Rh_3Se_2]^{2+}$ clusters is to be regarded as thermodynamically preferred pathway of cluster formation in the presence of Se^{2-} and $\{CpRh\}^{2+}$ source, irrespective of the *substituents* at Cp and selenide sources. ^{77}Se chemical shifts can be reliably calculated and can be used in the future to monitor formation of selenide clusters. Bonding situation in $[Cp^*_3Rh_3Se_2]^{2+}$ and in $[Cp^*_3Rh_3Se_2]^{2+}$ does not confirm to simplified electron counting schemes based upon 18 e rule: it involves participation of lone pairs of capping Se in the 2+ species effectively eliminating M–M bonding in formally 48 e species, and restores this bonding in the reduced, formally 50 e neutral species, by sacrificing the hapticity of M–Cp coordination. Reduction of hapticity to *2* and *3* upon two-electron reduction of $[Cp^*_3Rh_3Se_2]^{2+}$ provides extra coordination space necessary for CO_2

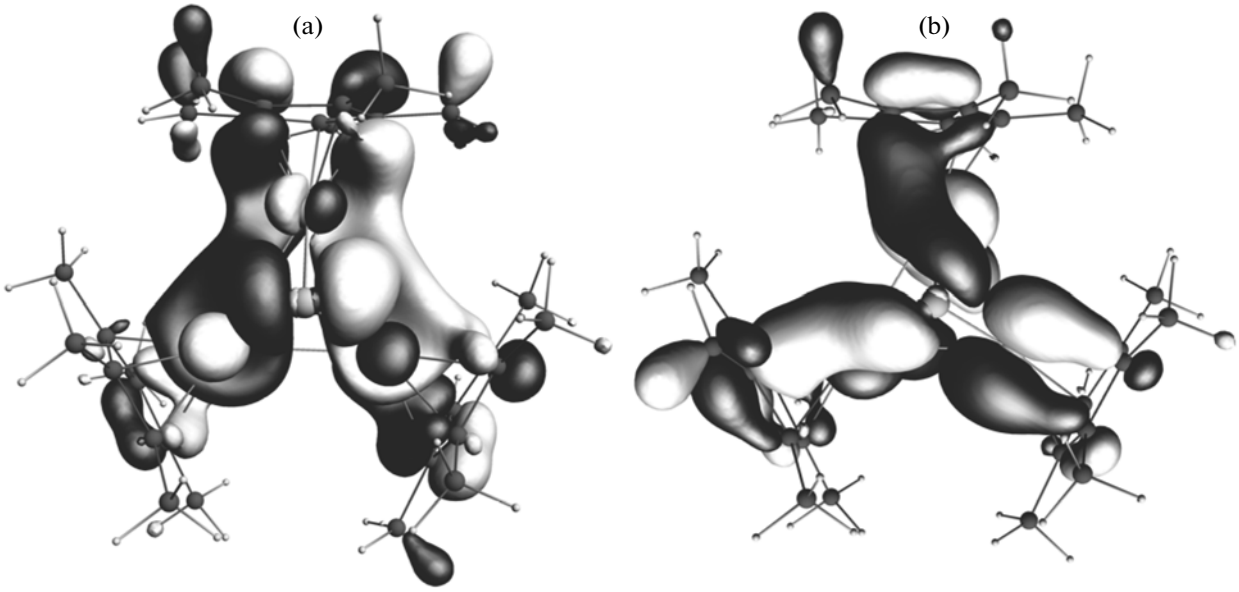

Fig. 5. MOs in $[Cp^*_3Rh_3Se_2]^{2+}$ cation: (a) HOMO (twice degenerated); (b) $HOMO^{-1}$.

Table 4. Properties of selected electron density critical points (a.u.)

Parameter	ρ	Δ	$\|V\|/G$	H
		$[Cp^*_3Rh_3Se_2]^{2+}$		
		BCP		
Rh–Se	0.0822	0.1249	1.4584	–0.0264
	0.0812	0.1242	1.4534	–0.0258
Rh–C	0.0761–0.0814	0.1984–0.2065	1.2650–1.3013	–0.0186...–0.0218
		RCP		
Rh–Se–Rh–Se	0.0385	0.0658	1.3018	–0.0071
Rh–C–C	0.0741–0.0770	0.2174–0.2279	1.2260–1.2325	–0.0159...–0.0171
Cp*	0.0480	0.2990	0.9659	0.0025
		CCP		
Rh–Rh–Rh–Se–Se	0.0317	0.0904	1.1066	–0.0027
Rh–Cp*	0.0460	0.2622	0.9818	0.0012
		$[Cp'_3Rh_3Se_2]^{2+}$		
		BCP		
Rh–Se	0.0822–0.0827	0.1240–0.1253	1.4630–1.4599	–0.0264...–0.0267
	0.0811–0.0819	0.1240–0.1245	1.4528–1.4580	–0.0257...–0.0262
Rh–C	0.0752–0.0822	0.1982–0.2081	1.2593–1.3051	–0.0181...–0.0223
		RCP		
Rh–Se–Rh–Se	0.0390	0.0660	1.3083	–0.0074
	0.0381	0.0662	1.2935	–0.0069
	0.0378	0.0662	1.2896	–0.0067
Rh–C–C	0.0739–0.0782	0.2166–0.2324	1.2253–1.2350	–0.0158...–0.0177
Cp'	0.0480	0.2987	0.9661	0.0025
	0.0480	0.2985	0.9660	0.0025
	0.0479	0.2979	0.9665	0.0024
		CCP		
Rh–Rh–Rh–Se–Se	0.0317	0.0905	1.1047	–0.0026
Rh–Cp'	0.0461	0.2629	0.9820	0.0012
	0.0461	0.2632	0.9817	0.0012
	0.0459	0.2610	0.9819	0.0012
		$[Cp^*_3Rh_3Se_2]^{0}$		
		BCP		
Rh–Se	0.0808	0.1187	1.4586	–0.0251
	0.0806	0.1186	1.4581	–0.0251
	0.0780	0.1173	1.4505	–0.0240
	0.0804	0.1182	1.4576	–0.0249
	0.0804	0.1187	1.4563	–0.0249
	0.0776	0.1167	1.4495	–0.0238
Rh–Rh	0.0436	0.0683	1.3489	–0.0091
	0.0422	0.0678	1.3341	–0.0085
Rh–C	0.0708–0.0847	0.2112–0.2187	1.2249–1.3018	–0.0156... –0.0235

Table 4. (Contd.)

Parameter	ρ	Δ	$\|V\|/G$	H
		RCP		
Rh–Se–Rh	0.0419–0.0431	0.0745–0.0778	1.2967–1.2986	–0.0079...–0.0082
Rh–C–C	0.0702–0.0764	0.2207–0.2410	1.2049–1.2174	–0.0142...–0.0166
	0.0663	0.2164	1.1846	–0.0122
	0.0767	0.2312	1.2265	–0.0170
	0.0781	0.2389	1.2270	–0.0175
	0.0627	0.2043	1.1819	–0.0114
	0.0811	0.2522	1.2295	–0.0188
Cp*	0.0477	0.2941	0.9633	0.0026
		CCP		
Rh–Cp*	0.0456	0.2570	0.9813	0.0012
	0.0453	0.2523	0.9832	0.0010
	0.0450	0.2483	0.9843	0.0010

coordination and eventual reduction in the electrocatalytic reaction.

ACKNOWLEDGMENTS

We thank Dr. C. Vicent (Serveis Centrals d'Instrumentacio Cientifica (SCIC) of the Universitat Jaume I, Castellon, Spain) for ESI–MS experiments. This work was partially supported by grant of FFP "SSESIR 2009–2013" no. 16.740.11.0598.

REFERENCES

1. Kushi, Y., Nagao, H., Nishioka, H., et al., *J. Chem. Soc., Chem. Commun.*, 1995, p. 1223.
2. Kushi, Y., Nagao, H., Nishioka, H., et al., *Chem. Lett.,* 1994, p. 2175.
3. Tanaka, K., Kushi, Y., and Tsuge, K., *Inorg. Chem.*, 1998, vol. 37, p. 120.
4. Tang, Zh., Nomura, Y., Ishii, Y., et al., *Organometallics*, 1997, vol. 16, p. 151.
5. Abramov, P.A., Sokolov, M.N., and Virovets, A.V., *J. Struct. Chem.*, 2009, vol. 50, p. 162.
6. Rowen, M., Churchill, S., and Julis, A., *Inorg. Chem.*, 1977, vol. 16, p. 1488.
7. ADF2008. SCM. Theoretical Chemistry. Amsterdam. http://www.scm.com
8. Becke, D., *Phys. Rev. A: Gen. Phys.*, 1988, vol. 38, p. 3098.
9. Perdew, J.P., *Phys. Rev. B: Condens. Matter*, 1986, vol. 33, p. 8822.
10. Vosko, H., Wilk, L., and Nusair, M., *Can. J. Phys.*, 1980, vol. 58, p. 1200.
11. Schreckenbach, G. and Ziegler, T., *J. Phys. Chem.*, 1995, vol. 99, p. 606.
12. Lenthe, E., Ehlers, A.E., and Baerends, E.J., *J. Chem. Phys.*, 1999, vol. 110, p. 8943.
13. Bader, R.F.W., *Atoms in Molecules. A Quantum Theory*, Oxford: Oxford Univ., 1990.
14. Becke, A.D. and Edgecombe, K.E., *J. Chem. Phys.*, 1990, vol. 92, p. 5397.
15. Savin, A., Jepsen, O., Flad, J., et al., *Angew. Chem., Int. Ed. Engl.*, 1992, vol. 31, p. 187.
16. Grabowski, J.S., *Monatsh. Chem.*, 2002, vol. 133, p. 1373.
17. Palusiak, M. and Krygowski, T.M., *Chem. Eur. J.*, 2007, vol. 13, p. 7996.
18. Silvi, B., *J. Mol. Struct.*, 2002, vol. 614, p. 3.
19. Feliz, M., Llusar, R., Andrés, J., et al., *New J. Chem.*, 2002, vol. 26, p. 844.
20. Andrés, J., Berski, S., Feliz, M., et al., *C. R. Chimie*, 2005, vol. 8, p. 1400.
21. Andres, J., Feliz, M., Fraxedas, J., et al., *Inorg. Chem.*, 2007, vol. 46, p. 2159.
22. *SHELXTL. Version 6.12. Bruker Advanced X-Ray Solutions*, Madison: Bruker AXS Inc., 2004.
23. *APEX2 (version 1.08), SAINT (version 7.03), SADABS (version 2.11). Bruker Advanced X-Ray Solutions*, Madison: Bruker AXS Inc., 2004.
24. Sokolov, M.N., Abramov, P.A., Peresypkina, E.V., et al., *Polyhedron*, 2008, vol. 27, no. 15, p. 3259.
25. Bereau, V. and Ibers, J.A., *C.R. Acad. Sci., Ser. IIc: Chim.*, 2000, vol. 3, p. 123.
26. Sokolov, M.N., Gushchin, A.L., Naumov, D.Yu., et al., *Inorg. Chem.*, 2005, vol. 44, p. 2431.
27. Espinosa, E., Alkorta, I., Elguero, J., and Molins, E., *J. Chem. Phys.*, 2002, vol. 117, p. 5529.
28. Galli, D., Garlschelli, L., Ciani, G., et al., *J. Chem. Soc., Dalton Trans.*, 1984, p. 55.
29. Antipin, M.Yu., Slovokhotov, Yu.L., and Struchkov, Yu.T., *Dokl. Akad. Nauk SSSR*, 1987, vol. 286, p. 1143.
30. Pasynski, A.A., *Russ. J. Coord. Chem*, 2011, vol. 37, p. 801.